

CORNELL NEURONEX

Technology Hub

2018 REU Research Papers



Pictured left to right: Anna Alvarez, Rick Zirkel, Nathan Barkdull, Kelsey Walker





High Speed Linear Raster Scanners for Use in COMPMRI

Anna Alvarez, Najva Akbari, Chris Xu

ABSTRACT: Functional Magnetic Resonance Imaging (fMRI) is one of the most widely used and studied techniques for imaging of the brain. However, as it cannot directly read neural synapses and cannot be used to image at the cellular level, fMRI alone does not provide enough information to give clear conclusions on a subject's brain. To resolve this, we propose a multimodal approach called Concurrent MultiPhoton microscopy and Magnetic Resonance Imaging (COMPMRI). By using fMRI and three photon microscopy simultaneously on mice, it will be possible to receive full brain scans and read neural activity at cellular regions at the same time. In this work, we present piezo driven, high speed linear raster scanners that can be used for three photon microscopy. Our scanners are MRI safe, have a field-of-view (FOV) of 143.5 by 62.96 μm , a resonant frequency above 423 Hz, and are capable to scanning at 256 lines/frame. While improvements must be made, results indicate our scanners can be used for in future studies for noninvasive COMPMRI imaging.

INTRODUCTION

Multiphoton microscopy and Functional Magnetic Resonance Imaging (fMRI) both present a promising future for advancements in brain imaging and understanding its functions. Multiphoton microscopy is regularly used for cellular imaging with high temporal resolution. fMRI, in turn, provides full brain scans with the highest spatial resolution for a noninvasive technique [1]. However, fMRI does not directly read neural synapses. Rather, it reads a secondary response: changes in blood flow due to neural activity. Therefore, any inferences made from fMRI results must rely on neurovascular coupling, or the relationship between neural activity in the brain and changes of cerebral blood flow [2]. Because this relationship is not a simple one, fMRI alone cannot be used to draw decisive conclusions. For example, during stimulation, regions of neural activity and haemodynamic responses may be noncontiguous; neurons from one location of the brain can be responsible for changes in oxygen levels in a different brain region. As seen in Figure 1, blood flow is also shown to stop before neurons cease firing. This demonstrates that increases in

oxygenated blood flow alone is not indicative of areas and intensities of neural firings.

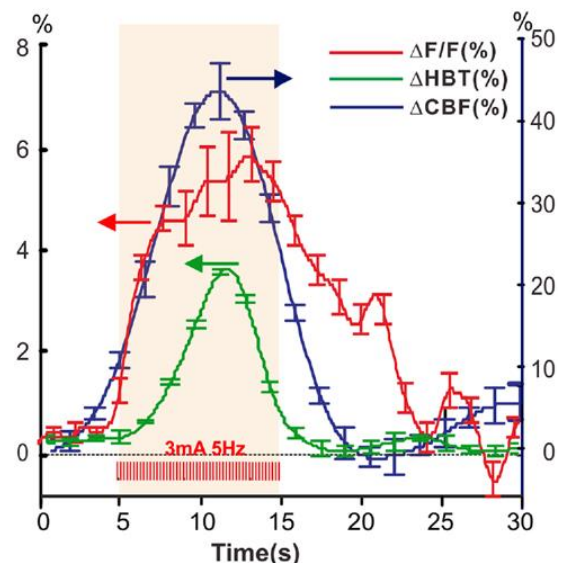


Figure 1: Cerebral blood flow (CBF), in blue, is shown to end before fluorescence intensities of dyed neurons, in red, die down in an HP stimulation. HBT signifies the amount of hemoglobin present [3].

It is difficult to draw good conclusions solely on fMRI or multiphoton microscopy. Thus, a multi-modal approach is needed. For small scale testing on mice, we propose COncurrent MultiPhoton microscopy and Magnetic Resonance Imaging (COMPMRI) as a solution. Combining fMRI with three photon microscopy in a multimodal approach, it will be possible to locate regions of activity in the brain and read both BOLD signals and neural activity simultaneously. Three-photon microscopy will be used due to its long excitation wavelengths, allowing high resolution imaging in subcortical layers of the mouse brain without the need of surgically removing the skull. This enables noninvasive in vivo imaging of the mouse brain and penetration up to 1400 micrometers [4].

Often when taking such a multimodal approach, the challenge is in simultaneously recording data using two instruments without having reduction in data quality [1]. For example, in the common combination of EEG fMRI with an MRI scans, metal inside the EEG will cause magnetic field distortions [1]. This in turn deforms the MRI results. To avoid such complications, all COMPMRI components inside of the MRI room must be magnetic field safe. While the laser itself can be housed in the control room, the lenses, casing, and XY scanner will be exposed to the magnetic field. Of these three, only the scanner and the housing compartment are traditionally metallic. A different material can easily be used to build a casing; the scanner, on the other hand, must be redesigned. Developing an efficient and compatible XY scanner has been the focus of this study.

Our XY scanners are composed of an optic fiber to deliver light, a carbon fiber tube (CFT) extension to amplify movements, and an actuator. For the linear raster scanners, trimorph piezoelectrics were chosen to drive the actuator, as piezos have already been shown to create negligible effect on magnetic fields [5]. Previous studies by Harzic RL et al. [6] and Rivera DR et al.[7] have created successful piezo driven XY scanners demonstrating a uniform FOV. Lastly, trimorph piezos produce more deflection compared to bimorph piezos [8][9], making them the ideal piezo type to use in our scanners.

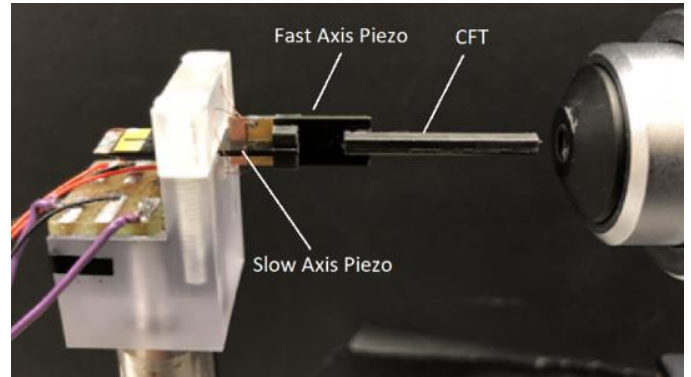


Figure 2: Image of experimental setup displaying how scanner components are attached and how an imaging lens is positioned relative to this setup.

The acquisition speeds of our piezo driven actuators are limited by the scanner's resonant frequency. For a linear scanner to function properly, changes in fiber tip deflection must be directly proportional to increases in applied voltage. This is represented by the linear region in Figure 3. Once the actuator approaches resonance, this relationship ceases to be linear. Resulting images become distorted and difficult to control; it is therefore essential that the resonance frequency be set as high as possible for a functional linear scanner. Frequencies of 500 Hz and above are considered high enough for good optical imaging. Thus, to enable imaging at this frequency range without interference, the scanner's resonance frequency must be far above 500 Hz.

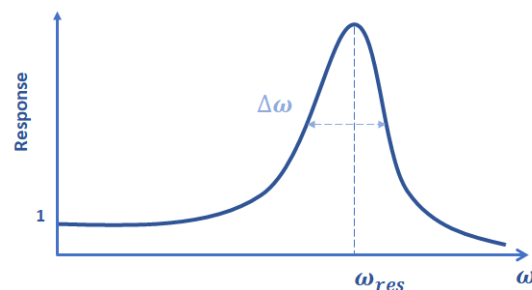


Figure 3: The relationship between amplitude of deflection and frequency (ω).

EXPERIMENTAL

The goal of these experiments was to maximize resonant frequencies of our scanners. Resonance frequencies were tested at three stages: when the scanner consisted of only a fast axis piezo,

when the CFT extension was attached to this piezo, and when the final slow axis piezo was added. As evident by Equation 1, increasing the Young Modulus, decreasing density, or decreasing cross sectional areas improves resonance frequency [10].

$$f_n = \frac{\beta_n^2}{2\pi L^2} \sqrt{\frac{EI}{\rho A}} \quad (1)$$

Here, E is Young’s Modulus, ρ is density, I is moment of inertia, A is cross sectional area, L is piezo overhang, and β is a boundary condition dependent constant [10]. Therefore, in a second experiment, three scanners with varying CFT diameters and densities were tested and measured for resonant frequency and linearity. The dimensions and densities of the CFTs used are recorded in Table 1. As cross-sectional area decreases, so did density, which in theory will greatly increase resonant frequency.

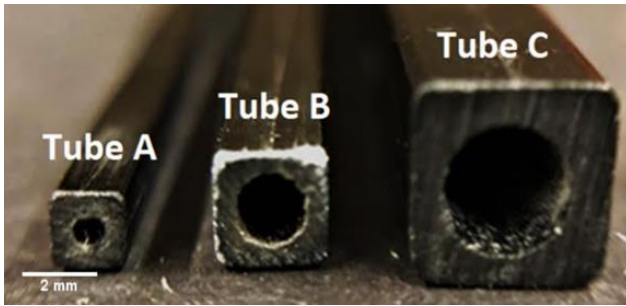


Figure 4: CFTs of increasing density and cross-sectional area from left to right.

Carbon Tube	Dimensions (mm)	Density (oz/mm)
Tube A	Autek 2x2x1 ID	0.00017350
Tube B	Autek 3x3x2 ID	0.0003125
Tube C	Midwest Products 4.9784x3.175x2 ID	0.000675

Table 1

Scanner Construction

To create our scanners, trimorphs and CFT were cut to fit the dimensions calculated using Equation 2 under Experimental Setup. Copper wiring was used to connect the piezoelectric layers to the circuit and the carbon fiber layer to ground. An optic fiber was glued onto the CFT with little or no overhang. During construction, it was critical that all elements be aligned parallel, else the abnormalities would affect the final resonance and imaging. The fast axis piezo, as labeled in Figure 2, was mounted with the desired overhang, and the CFT was glued in parallel to this. Once complete, the setup was wired to the circuit and driven with a sinusoidal wave to test for resonance. Resonance was determined by examining the changes in fluctuation under a microscope. Linearity was also tested by measuring deflection of the CFT tip due to offset changes made by a function generator. The slow axis piezo was prepared by cutting a notch through the trimorph’s end and fitted perpendicularly with the first trimorph. With this orientation, the fast and slow axis piezo allowed for movement in the X and Y direction respectively. CFT reinforcements were glued by this connection for stability. Linearity and resonance were calculated once more.

Experimental Setup

In a trimorph piezo, two piezoelectric layers are separated by a carbon-fiber layer [8]. To induce deflection, one piezoelectric side must experience a positive voltage while the other is grounded [8]. Simply feeding the scanner a triangular wave will result in a negative voltage input for half the time. A circuit was constructed to divide the pattern and invert negative values, as shown in Figure 5. By adjusting the resistance values in the circuit, the voltage gain could also be manipulated. Trimorphs used in this study can receive a maximum voltage of 200 Vpp. Achieving a final voltage of this value is ideal, as it results in maximum deflection and the largest FOV.

To test resonance and linearity, a function generator provided a sinusoidal wave. This was fed into the circuit and then a linear amplifier to increase gain by 25. When testing linearity, the tip of the scanner was projected onto a computer screen using an optical microscope camera. Power supplies and

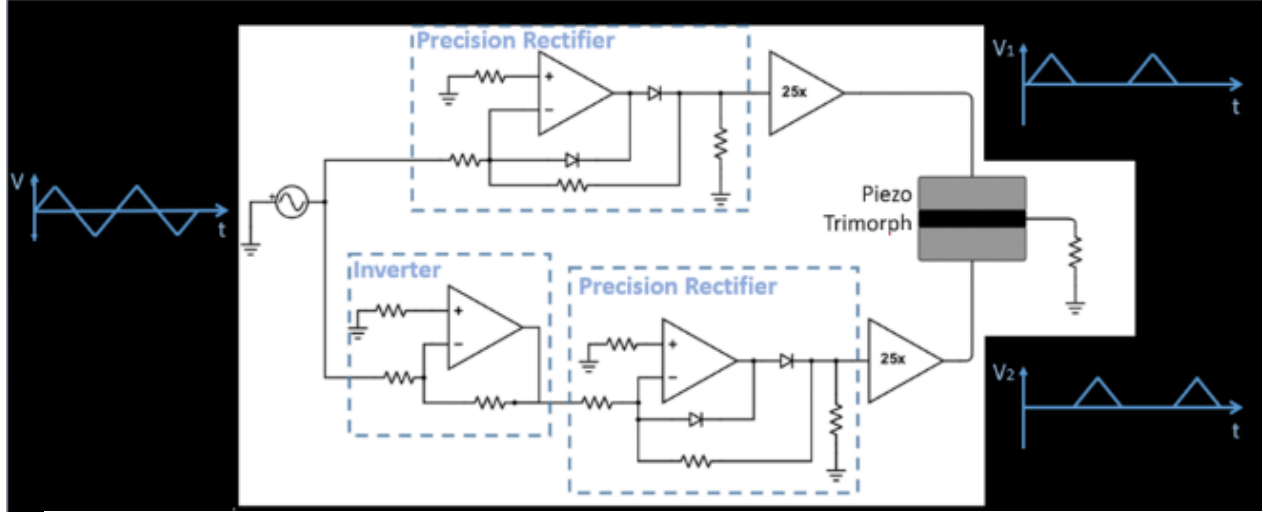


Figure 5: Schematic of circuit constructed. Positive and negative voltages are fed to separate piezoelectric sides of a trimorph.

the piezo drive were activated. Frequency on the function generator was set to 0, the amplitude set to 7 V_{pp}, and the offset initially set to 0 V_{dc}. The starting position of the tip was marked. The offset was then increased by increments of 0.5 V_{pp} in both positive and negative directions. After each shift, the new tip position was recorded. Pixel distances between each position were measured and converted to micrometers.

To test resonance, the scanner was projected on the computer screen in a similar fashion. Frequency was initially set to 50 Hz and increased in increments of 10 Hz. Amplitude was set to 800 mV, and offset returned to 0 V_{dc}. An increase in frequency results in scanner tip oscillations, evident in the vibrations seen on the computer screen. Frequency was increased until vibrations were maximized, indicating the scanner had reached resonance.

To determine the optical overhang lengths of the piezos, the following equation was used:

$$D = 2c(L_1^2 + 2L_1L_2) \times \left(\frac{V_{\text{applied}}}{V_{\text{spec}}} \right), \quad (2)$$

Here, D is fiber tip deflection at a non-resonant frequency and c is a proportionality constant. L_1 and L_2 are the slow and fast axis trimorph overhangs respectively [7]. With this equation as our guideline, we found that a fast axis overhang of 10 mm, a slow axis overhang of 7 mm, and a CFT overhang of 20

mm would provide a fiber-tip deflection of approximately 900 μm at 200 V_{pp}. To improve resonance, we chose to alter the fast axis to have an overhang length of 9 mm instead.

RESULTS AND DISCUSSION

For the first experiment, the resonant frequencies and total fiber tip displacement of a scanner at its three stages were recorded in Table 2. There is an unavoidable trend of decreasing resonance as the scanner becomes longer with each new addition. The displacement, indicative of FOV, is also seen to increase with each new addition.

Results of the second experiment are recorded in Table 3. Each scanner, containing a varying CFT, was built to its second stage. Density of the CFTs increased with its outer diameter, and as Equation 1 suggests, scanners built with denser CFTs have a lower resonant frequency. The total deflections of the scanners appear similar with 3 mm and 5 mm CFTs, but is largely reduced when built with a 2 mm CFT. This demonstrates a nonlinear relationship and must be further investigated with more data points.

	Stage 1	Stage 2	Stage 3
Resonance (Hz)	3970	633	Fast: 610 Slow: 394
Total Deflection (μm)	28.08	94.36	Fast: 775.1 Slow: 279.4

Table 2

	Tube A 2 mm	Tube B 3 mm	Tube C 5 mm
Resonance (Hz)	1040	522	309
Total Deflection (μm)	277.5	678.1	607.8

Table 3

A complete scanner was constructed using the 3 mm CFT and with the dimensions calculated using Equation 2. While the 3mm CFT scanners do not have the largest resonant frequency, they have a much larger FOV than scanners with 2 mm CFTs. The piezoelectric linearity characterizations of its piezos are graphed in Figures 6 and 7. The first graph depicts both sides of the fast axis piezo's deflection. The second depicts the same information for the slow axis piezo. As these two graphs are not identical, the scanner cannot image the same amount in the X and Y direction. Further, the graph demonstrates that the two trimorph piezoelectric sides perform differently. The linearity equations vary when the trimorph is initially receives a positive or negative voltage. This implies scans lines taken left to right are not identical to scan lines taken right to left.

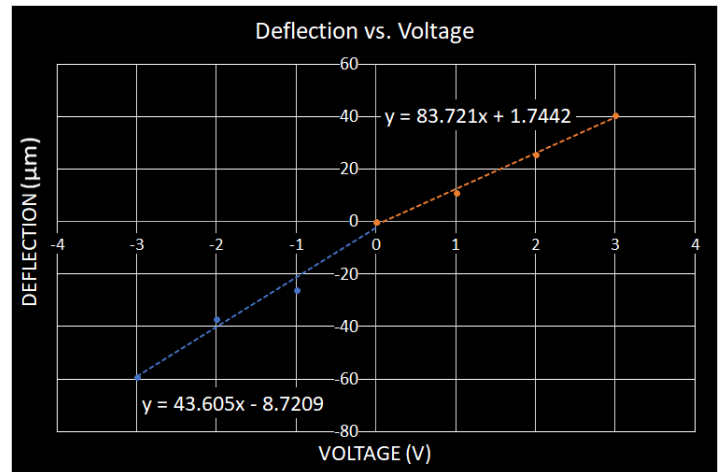


Figure 7: Linearity characterization of the fast axis piezo from a complete scanner. 3mm CFT with 20 mm overhang, fast axis overhang of 9mm, slow axis overhang of 7mm.

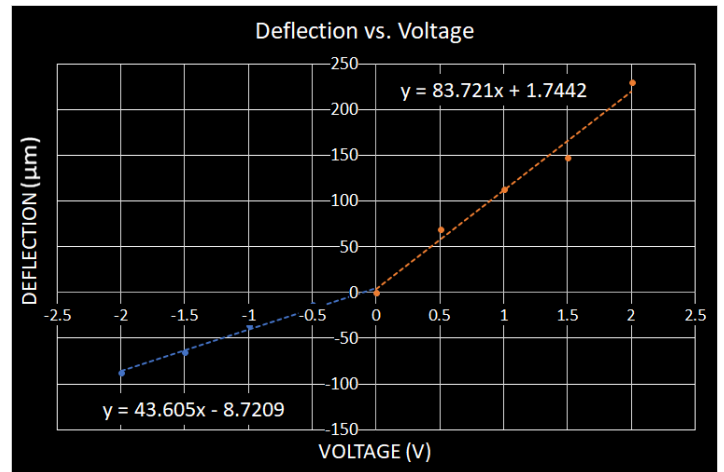


Figure 6: Linearity characterization of the slow axis piezo.

To verify this, the scanner was tested on an airforce-target using a 980nm laser diode. The fast axis was scanned at a frequency of 423.7 Hz, and the slow axis was scanned at 256 lines/frame. The resulting image, Image I, is shown in Figure 6. By feeding this image through MATLAB, the left to right and right to left scan lines taken from each trimorph side were separated. These images are shown side by side with noticeable variations between the two. For example, Image II captures more of the air force target scan pattern below, while Image III captures more of the leftmost pattern. When combined, resulting image is of low resolution.

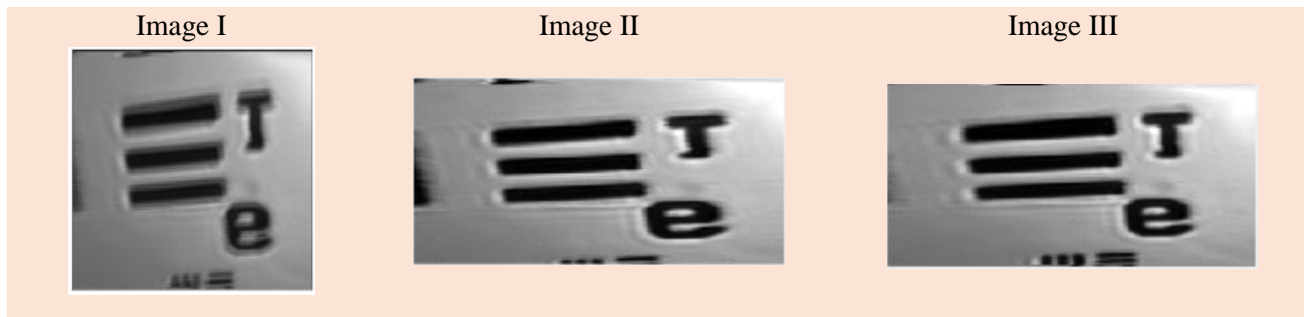


Figure 8 I: Complete image taken with scanner via ScanImage. II: Left to right scan lines III: Right to left scan lines.

CONCLUSION

Thus far, complete scanners have only been tested successfully at frequencies ranging from 400 to 500 Hz. However, their scanning acquisition speeds do not exceed the performance of most other commercially available actuators today. Further work must be done to improve resonance frequencies. As for linearity characterizations, each of the trimorph's piezoelectric sides have been demonstrated a varying voltage to displacement relationship, resulting in a non-uniform FOV. To resolve this, an arbitrary waveform generator that corrects for this response must be installed for future testing.

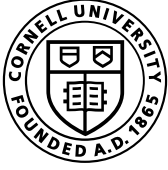
ACKNOWLEDGMENTS

I would like to thank Chris Xu, Navja Akbari, and the Xu Research group for their help and support on this project throughout the summer. I would also like to thank NSF, NIH, and the NeuroNex REU for funding.

REFERENCES

- [1] Uludağ K, Roebroek A. General overview on the merits of multimodal neuroimaging data fusion. *NeuroImage*. 2014;102:3-10. doi:10.1016/j.neuroimage.2014.05.018
- [2] Logothetis NK. What we can do and what we cannot do with fMRI. *Nature*. June 2008. doi:10.1038/nature06976
- [3] Gu X, Chen W, et al. Long-term optical imaging of neurovascular coupling in mouse cortex using GCaMP6f and intrinsic hemodynamic signals. *NeuroImage*. September 2017. doi:10.1016/j.neuroimage.2017.09.055
- [4] Xu C. In vivo multiphoton imaging of subcortical structures in an intact mouse brain. *Frontiers in Optics 2012/Laser Science XXVIII*. 2012. doi:10.1364/fio.2012.fw5c.5
- [5] Wang Y, Cole G, et al. MRI compatibility evaluation of a piezoelectric actuator system for a neural interventional robot. *2009 Annual International Conference of the IEEE Engineering in Medicine and Biology Society*. September 2009. doi:10.1109/iembs.2009.5334206
- [6] Harzic RL, Weinigel M, et al. Nonlinear optical endoscope based on a compact two axes piezo scanner and a miniature objective lens. *Optics Express*. 2008;16(25):20588. doi:10.1364/oe.16.020588
- [7] Rivera DR, Brown CM, Ouzounov DG, et al. Compact and flexible raster scanning multiphoton endoscope capable of imaging unstained tissue. *Proceedings of the National Academy of Sciences*. 2011;108(43):17598-17603. doi:10.1073/pnas.1114746108
- [8] Milojević A, Tomić M, et al. Experimental Investigation and Modeling of Piezoelectric Actuator Behaviour for Transport Applications. Paper presented at: The Sixth International Conference Transport and Logistics; 26 May 2017; Niš, <http://til.masfak.ni.ac.rs/images/til-pedja/6.6.pdf> Accessed August 3, 2018
- [9] Nestorović T, Marinković D, et al. Modeling of piezoelectric smart structures by implementation of a user defined shell finite element. *Facta Universitatis - series Mechanical Engineering*. 2013;11:1 -12.

[10] University of Connecticut School of Engineering.
Module 10: Free Vibration of an Undamped 1D
Cantilever Beam.
http://www.engr.uconn.edu/~cassenti/AnsysTutorial/Modules_APDL/Module%2010_Vibrations.pdf Accessed
August 4, 2018.



Immunohistochemistry of Hsp70 in *Drosophila Melanogaster* to Validate the Procedure of Three-Photon Microscopy

Nathan Barkdull¹, Max Aragon², and Nilay Yapici²

¹ Department of Physics, University of Florida, Gainesville, FL, 32611

² Department of Neurobiology and Behavior, Cornell University, Ithaca, NY, 14853

Abstract: Three-photon microscopy provides neuroscientists a powerful tool to capture neural dynamics while the animal of interest is conducting a behavior task. In the study of *Drosophila melanogaster*, the development of this imaging technique would enable non-invasive chronic imaging of neural circuits as flies change physiologic and behavioral states. In this study, we demonstrated that the three-photon imaging procedure does not affect levels of Hsp70 in brain tissue, an indicator of stress, heating, and photo-damage, using immunohistochemistry. Our results suggest that the laser power used during three-photon microscopy of the fly brain does not affect the behavior or neural dynamics of imaged flies.

Introduction

Intricate neurological processes serve as the basis for complex behaviors and decision making in all animals. Behavior and underlying neural function change as an animal ages and experiences the world: increasing amyloid plaques in aged primate's brains leads to decreased agility and movement, increased anxiety responses in older mice when introduced to new environments, and cyclical behavior changes in flies caused by clock neurons relaying time of day [1][2][3]. The fruit fly *Drosophila Melanogaster* is genetically tractable and exhibits a wide range of behaviors and is thus amenable to studying the neural correlates of behavior via imaging techniques like two-photon microscopy. Imaging the fly brain with this technique, however, requires removing the head cuticle, layers of fat tissue, and trachea. This process typically kills the fly within five hours, which gives neuroscientists a short window in which to study neural function thus preventing the study long-term behavioral and physiological changes [4].

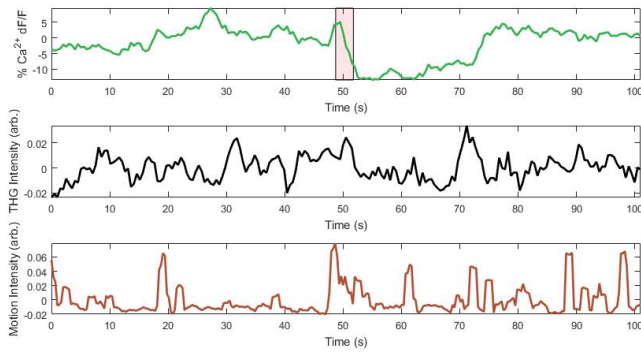
The development of a non-invasive procedure is therefore required to study chronic neural processes. Three-photon microscopy is a possible method, and although largely unexplored in fly neuroscience research, has several advantages over traditional imaging methods. Due to the heterogeneity of brain tissue, light entering the brain typically becomes scattered, resulting in a high signal to background ratio which limits the applicability of traditional imaging techniques. Multiphoton microscopy (MPM) utilizes multiphoton excitation, wherein multiple lower wavelength photons can be simultaneously absorbed by a fluorophore that would normally only be excited by a single photon of higher energy [5]. The probability of this

simultaneous quantum event is extremely low, so it is important to maintain a high excitation photon flux, generally achieved using femtosecond pulsed lasers [6]. Since MPM employs excitation photons of a longer wavelength and losses due to scattering decrease proportional to λ^{-4} , imaging depth is increased to a point where *in vivo* imaging through the cuticle of *Drosophila* with subcellular resolution is possible using this longer wavelength imaging [4]. Additionally, the non-linearity of MPM allows for optical sectioning, since excitation can be maintained within the focal plane, decreasing background noise as the probability of absorption drops off rapidly as distance from the focal plane increases [7].

In biological imaging three-photon microscopy (3PM) has advantages over the more commonly used two-photon setup. Due to the ability to use photons with a third of the excitation energy, 3PM benefits from further reduced scattering. The higher order nonlinearity results in improved signal to background ratio and subsequently, greater imaging depth [8]. In mice, 3PM has already been used to create a method for deep, high resolution, non-invasive imaging that was not previously possible with two photon systems [9] and it was recently shown in *Drosophila* that 3PM can resolve single neurons *in vivo* through an intact cuticle [4].

Despite these advancements and advantages, chronic studies with 3PM in *Drosophila* have yet to be explored outside of the Yapici lab. 3PM experiments studying odor responses as flies become increasingly starved demonstrate that chronic imaging through the cuticle is possible. Preliminary results suggest that neural activity reported by the calcium indicator GCaMP6s increases as a fly becomes hungrier over a ten-hour starvation period (Figure 1).

Odor Response at 0th hour



Odor Response at 10th hour

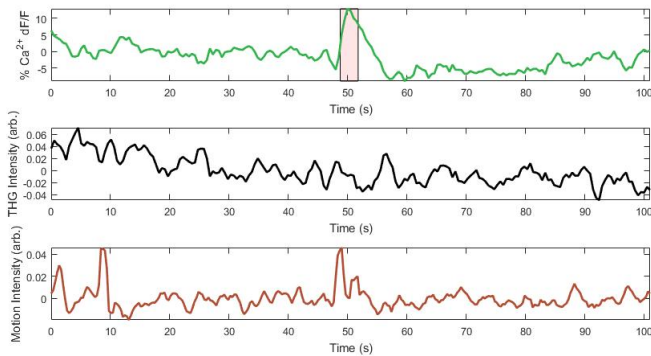


Figure 1: Transcuticular three-photon imaging of odor-evoked responses in the neurons of the mushroom body. Highlighted region of the Ca²⁺ graph shows the three second odor stimulus, created by passing compressed air through reservoir of apple cider vinegar. Calcium dynamics show change in response after significant period without food.

Although these results show that transcuticular imaging using 3PM is possible, it remains unclear if short or long-term imaging induces heating or non-linear damage in the brain, or if imaging stresses the fly. Identifying signs of brain damage or stress is important as imaging-induced changes to an animal's behavioral and neural patterns will be difficult to distinguish from natural changes and will hence limit the insight provided by long-term neural and behavioral studies. Heating the brain can affect channel conductance, the waveform of nerve impulses, and at extreme levels, provoke inflammatory responses and cell death, all of which can affect behavior [10]. Non-linear photo damage can cause cells to lyse, create artificial spikes in Ca²⁺ and at high intensities damage DNA sufficiently to reduce cell division [11]. It would need to be established that the act of imaging neurons with this procedure, does not

affect their function for three-photon imaging to be an effective technique for neuroscientists.

When most organisms are subjected to environmental stresses, heat, pH change, toxic exposure, etc. expression of heat shock protein 70 (Hsp70) increases. This protein functions as a molecular chaperone protecting cellular processes and reversing damage [12]. Hsp70 reduces the agglomeration of misfolded proteins by binding to exposed hydrophobic regions and utilizing an ATP driven mechanism to restore native confirmation [13]. This protein has been used as a marker for photo damage in similar experiments which examined non-linear and heating damage caused by two-photon experiments on mice [14] [10]. These experiments identified thresholds above which significant heating damage would occur, suggesting the existence of similar limits for 3PM. Inspired by these results, Hsp70 was selected as a photo-damage and stress indicator for the fly brain. If low levels of Hsp70 were found in imaged flies it would suggest that heating, non-linear photo damage, and stress induced from 3P imaging are insubstantial, and may not affect long term neural function or behavior.

Methods

Fly Stocks

The *Drosophila melanogaster* strain 20XUAS-GCaMP6s; mef2Gal4 was used for histology, and all flies were between 2 and 5 days old upon dissection. Larvae and flies were raised in 25°C incubators on an agar, yeast, corn meal, and sucrose medium.

Fly Preparations

The procedure for three-photon imaging alone has the potential of being sufficiently stressful to the flies that it could prompt Hsp70 expression without the use of the laser. It is therefore important to test all aspects of the imaging procedure to see if each may elicit a stress response that could obscure the Hsp70 expression in imaged flies. The current procedure first requires adhering the fly by its head to the underside of a coverslip with a UV curable liquid plastic. The coverslip is then attached to a plastic weighing dish which is mounted under the laser path during imaging. Chronic imaging necessitates that the fly be placed on a water ball which provides it the moisture necessary to survive the lengthy imaging. While imaging is occurring, the fly is illuminated by an IR lamp as motion data is collected by an IR camera. To test for stress induced from this procedure two groups of flies were mounted but not

imaged for a similar time period, with one of the groups left under an IR lamp for the duration to test the effects of IR lamp illumination on Hsp70 expression.

In addition to flies that had undergone imaging tests for ten minutes at 30 mW and a repetition rate of 1 MHz, four other preparations were created as positive and negative controls. Flies were starved and heat shocked, fed and heat shocked, starved without heat shock and fed without heat shock before dissections were performed. Heat shocking occurred for a period of one hour at 37°C, a duration and temperature sufficient to ensure Hsp70 expression in brain tissue [12].

Immunohistochemistry

For the controls, male flies were anesthetized with CO₂ prior to brain dissection and trachea removal, which then occurred in 1x PBS (phosphate-buffered saline). Brains were then fixed in 50 µl of 4% paraformaldehyde for one hour and incubated with agitation via an orbital shaker.

For imaged flies, after imaging was completed they were decapitated and fixed in paraformaldehyde for two-four

hours and then placed in PBS for short term storage prior to the dissection process (same as above).

After four fifteen-minute washes with 50 µl of PBT, gently agitated, brains were blocked with 50 µl of 5% NGS (normal goat serum) in PBT for one hour, gently agitated. Primary antibodies were then added, diluted in 5% NGS PBT solution, 50 µl of 1:20 anti-nc82 in mouse used to label the whole brain structure, 50 µl of 1:1000 anti-GFP in rabbit used to label the mushroom body structures, and 50 µl of 1:200 anti-Hsp70 in rat to label areas expressing heat damage. Brains were set on orbit shakers and left in 4°C cold room overnight to incubate. The following day, brains were rinsed five times in PBT, with gentle agitation, before secondary antibodies were added, 50 µl of 1:500 CY5 anti-mouse, 50 µl of 1:1000 488 Alexa Fluor anti-rabbit, and 50 µl of 1:1000 546 Alexa Fluor anti-rat. Brains were again set on orbit shakers and left in 4°C cold room overnight to incubate. The following day, after four fifteen-minute PBT washes with gentle agitation, one drop of VECTASHIELD antifade mounting medium was added to the brains. Following one hour of incubation on an orbital shaker, brains were mounted on a glass slide.

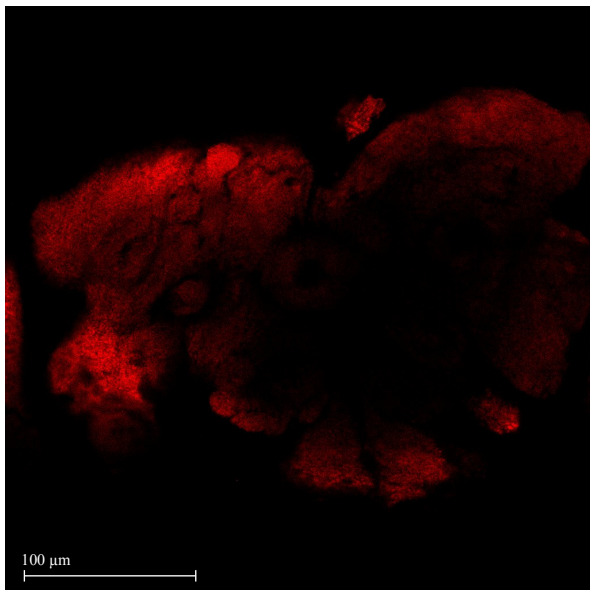


Figure 3: Image preparation for 24-hour duration

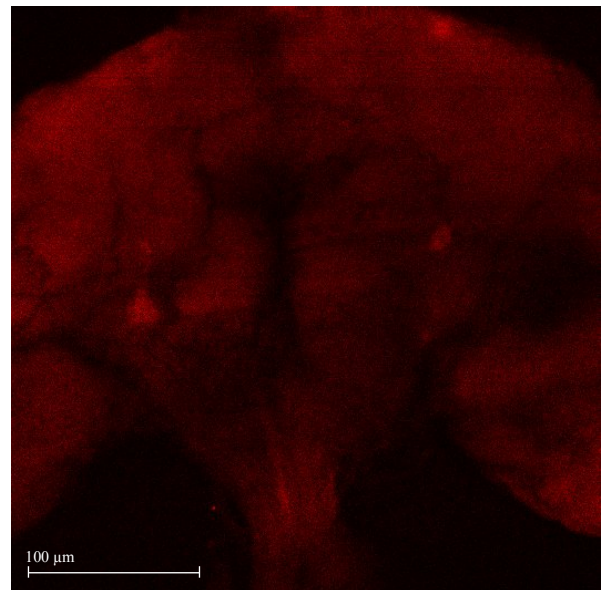


Figure 3: Image preparation, with IR lamp exposure for 24-hour duration

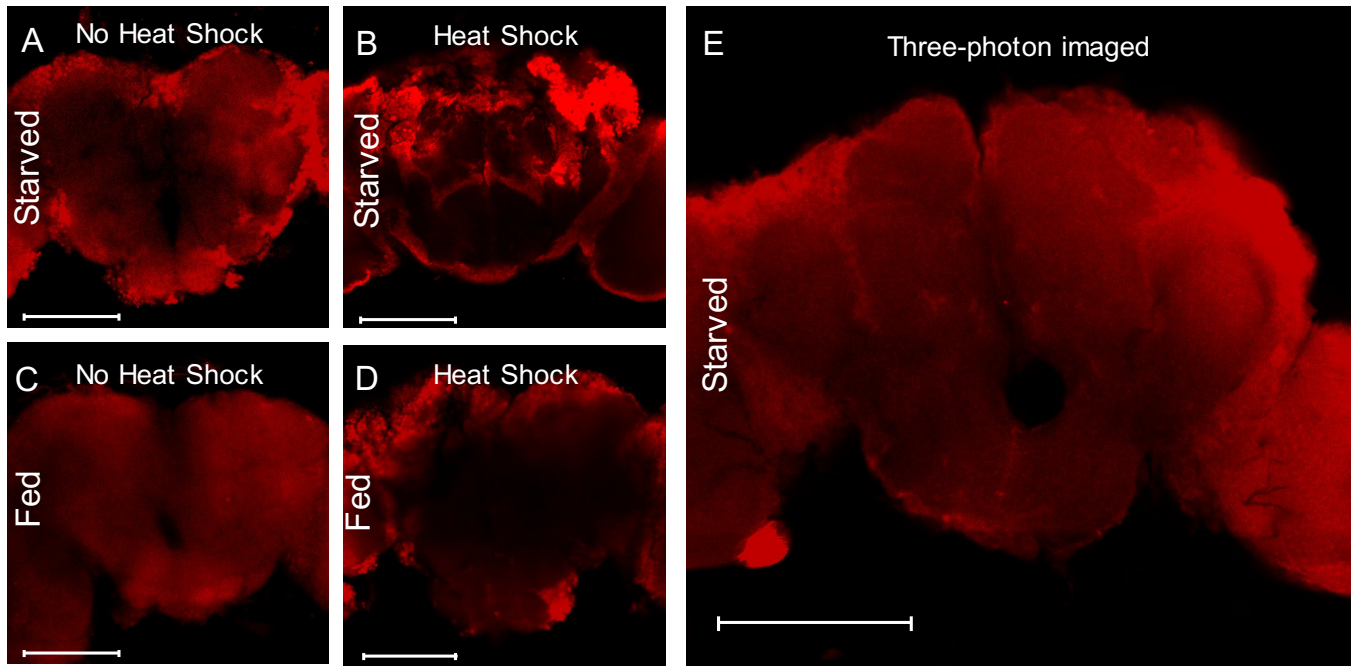


Figure 4. A. Negative control, fly starved 24-hours before dissection, little Hsp70 expression. B. Positive control, fly starved 24-hours and heat shocked for one hour at 37°C, significant Hsp70 expression. C. Negative control, fly fed prior to dissection, low Hsp70 expression. D. Positive control, fly fed prior to dissection and heat shocked for one hour at 37°C, significant Hsp70 expression. E. Three-photon imaged fly starved 24-hours, similar levels of Hsp70 expression as negative control. Scale bar = 100µm

Results

Brains were imaged by confocal microscopy at a resolution of 340 by 340 µm using laser light at 561 nm to excite labeled Hsp70. The negative control, 24-hours starved without heat shock, displays little Hsp70 expression. This level is suggested by the grainy signal received and little to no discernable cellular features conveyed by microscopy (Figure 4A). However, the positive control shows clear Hsp70 expression, as fluorescence levels are sufficient to reveal cellular features (Figure 4B). The 24-hour starved, and imaged brain shows low levels of detail suggesting that it is more similar to the negative control in its level of heat shock response (Figure 4E).

These levels of Hsp70 expression allow us to conclude that the imaging procedure on 24-hour starved flies results in no significant heating or non-linear damage in the fly brain. These results do not guarantee that the imaging procedure leaves the behavior of flies unaffected but provides one piece in a puzzle to understanding the full effects of *in vivo* 3PM imaging.

The two imaging preparations, with and without IR lamp exposure for 24-hours compare favorably against the controls, suggesting that the prep itself does not cause a stress response that evokes Hsp70 expression (Figure 2) (Figure 3).

Additional comparisons can be drawn between the starved and fed flies. It appears as though there is additional Hsp70 expression in flies that have been starved compared directly to their fed counterparts. For the purpose of our experiments however, this is not problematic. We expect that there will be behavioral differences between fed and starved trials. This is not an unexpected result as previous studies have shown in fish, that starvation period and Hsp70 expression form a linear relation [15].

Conclusion and Future Directions

Through this study, we have demonstrated that imaging flies using three-photon microscopy for a period of ten minutes at 30 mW and a repetition rate of 1 MHz, results in no significant expression of Hsp70 when compared to negative controls. There is no evidence of non-linear or

global heating damage as a result of the level of laser power necessary to complete transcortical imaging.

To build upon this body of work, it would be useful to study flies that had undergone an imaging period in excess of 12-hours. If it could be shown that this extreme case, which is the most likely to excite a stress response or create photo-damage in tissue, produces no alteration to behavior or increases Hsp70 expression it would be a strong indicator as to the reliability of three-photon imaging for chronic studies.

The conclusions of this study could be further reinforced by studying the behavior of flies after they have been imaged. If it could be shown that imaging has no effect on

the mating or feeding behaviors of flies, there would be behavioral evidence as to the nondestructive capabilities of three-photon imaging.

Acknowledgments

This work was supported by the Laboratory for Innovative Neurotechnology at Cornell and funded by the National Science Foundation NeuroNex grant (DBI-1707312) and Research Experience for Undergraduates program. I would like to thank Staci Thornton and Mengran Wang for aiding in imaging samples and Nilay Yapici and Max Aragon for their exceptional dedication and support over the duration of this project.

References

- [1] Bons, N., Mestre, N., & Petter, A. (1992). Senile plaques and neurofibrillary changes in the brain of an aged lemurian primate, *Microcebus murinus*. *Neurobiology of Aging*, 13(1), 99-105. doi:10.1016/0197-4580(92)90016-q
- [2] Shoji, Hirotaka, et al. "Age-Related Changes in Behavior in C57BL/6J Mice from Young Adulthood to Middle Age." *Molecular Brain*, vol. 9, no. 1, 2016, doi:10.1186/s13041-016-0191-9.
- [3] Grima, B., Chélot, E., Xia, R., & Rouyer, F. (2004). Morning and evening peaks of activity rely on different clock neurons of the *Drosophila* brain. *Nature*, 431(7010), 869-873. doi:10.1038/nature02935
- [4] Tao, X., Lin, H., Lam, T., Rodriguez, R., Wang, J. W., & Kubby, J. (2017). Transcortical imaging with cellular and subcellular resolution. *Biomedical Optics Express*, 8(3), 1277. doi:10.1364/boe.8.001277
- [5] Göppert-Mayer, M. (1931). Über Elementarakte mit zwei Quantensprüngen. *Annalen Der Physik*, 401(3), 273-294. doi:10.1002/andp.19314010303
- [6] Zipfel, W. R., Williams, R. M., & Webb, W. W. (2003). Nonlinear magic: Multiphoton microscopy in the biosciences. *Nature Biotechnology*, 21(11), 1369-1377. doi:10.1038/nbt899
- [7] Strickler, J. H., Webb, W. W., & Denk, W. (1991). Two-photon excitation in laser scanning fluorescence microscopy. *Science*, 248(4951), 73-76. doi:10.1117/12.47787
- [8] Ouzounov, D. G., Wang, T., Wang, M., Feng, D. D., Horton, N. G., Cruz-Hernández, J. C., . . . Xu, C. (2017). In vivo three-photon imaging of activity of GCaMP6-labeled neurons deep in intact mouse brain. *Nature Methods*, 14(4), 388-390. doi:10.1038/nmeth.4183
- [9] Horton, N. G., Wang, K., Kobat, D., Wise, F. W., & Xu, C. (2012). In Vivo Three-Photon Microscopy of Subcortical Structures within an Intact Mouse Brain. *Conference on Lasers and Electro-Optics 2012*. doi:10.1364/cleo_si.2012.cth5c.4
- [10] Podgorski, K., & Ranganathan, G. (2016). Brain heating induced by near-infrared lasers during multiphoton microscopy. *Journal of Neurophysiology*, 116(3), 1012-1023. doi:10.1152/jn.00275.2016
- [11] Hopt, Alexander, and Erwin Neher. "Highly Nonlinear Photodamage in Two-Photon Fluorescence Microscopy." *Biophysical Journal*, vol. 80, no. 4, Apr. 2001, pp. 2029-2036., doi:10.1016/s0006-3495(01)76173-5.
- [12] Ashburner, M., & Bonner, J. (1979). The induction of gene activity in *drosophila* by heat shock. *Cell*, 17(2), 241-254. doi:10.1016/0092-8674(79)90150-8
- [13] Mosser, D. D., Caron, A. W., Bourget, L., Meriin, A. B., Sherman, M. Y., Morimoto, R. I., & Massie, B. (2000).

The Chaperone Function of hsp70 Is Required for Protection against Stress-Induced Apoptosis. *Molecular and Cellular Biology*, 20(19), 7146-7159. doi:10.1128/mcb.20.19.7146-7159.2000

- [14] Kondo, M., Kobayashi, K., Ohkura, M., Nakai, J., & Matsuzaki, M. (2017). Two-photon calcium imaging of medial prefrontal cortex and hippocampus without cortical invasion. *ELife*. doi:10.1101/119404

- [15] Yengkokpam, S., et al. "Metabolic Modulation in *Labeo Rohita* Fingerlings during Starvation: Hsp70 Expression and Oxygen Consumption." *Aquaculture*, vol. 285, no. 1-4, 26 Aug. 2008, pp. 234-237., doi:10.1016/j.aquaculture.2008.08.034.

Developing a Method that Stabilizes Mice
for Spinal Cord Imaging,
While Maintaining a Normal Gait Cycle

Kelsey Walker

P.I. Chris Schaffer, Cornell University.

ABSTRACT

Spinal cord neural activity controls the limb motions that are necessary for locomotion. Essentially, spinal cord neurons fire to achieve continuous motion in vertebrates, but the problem is that the specific neurons that are responsible for these firings are not known. Correlating neural activity with specific locomotor patterns will aid in elucidating spinal locomotor circuitry. It is important for us to understand if there is a difference in gait patterns between tail held and spine fixed mice with surgical windows implanted on the spine. This question will be answered through conducting limb/gait video analysis of the 6 points of interest on a mouse's hind legs, including the Iliac crest, hip, knee, ankle, foot, and toe regions. During this study, when comparing tail-held to spine fixed, we have found that the 3 major points that are analyzed do not differ for more than 20 ° in angle differences. Although statistically, we can see that there is a change in patterns, it is vital to understand that each mouse is different, and many circumstances will affect the locomotion of a mouse.

INTRODUCTION

A plethora of neurodegenerative diseases like Alzheimer's disease, Parkinson's Disease, and Spinal Muscular Atrophy are associated with the interruption/disturbances of gait and limb movement in vertebrates. Gait is essentially sequential movements executed by motoneurons that is necessary for locomotion, which is the ability to move from one place to another. Gait is composed of two critical phases: the swing phase and the stance phase, which contributes to the routine step cycle. The stance phase is when the foot/ankle is not in contact with the ground, while the swing phase is when the foot/ankle is not in contact with the ground ¹. Locomotion can be perceived as an "effortless" function that accompanies vertebrates, but in reality, it is a highly complicated motor skill that relies on the activation of other limb and body muscles to produce a systematic routine that enables us to take steps ¹¹. The initiation of the locomotor functions takes place in the cortex ², basal ganglia ³⁻⁵, midbrain ⁶⁻⁷ and the hindbrain ⁸⁻¹⁰. However, the specific timing and locomotive patterns are accommodated by sensory neurons that are located in the

spinal cord tissue directly ¹¹⁻¹². These neurons fire to achieve locomotion, and we will record the activity of these neurons using a calcium indicator called GCaMP. We can observe neural activity via GCaMP fluorescence through a custom made surgical window that allows for long term optical access to the spinal cord ¹³. Previously, our lab has used two photon microscopy to visualize the spinal cord neurons, but we are currently transitioning to the usage of three photon microscopy, because it allows us to image much deeper structures in the the spinal cord tissue. It is important for us to understand if there is a difference in gait patterns between tail held and spine fixed mice with surgical windows implanted on the spine. We will answer this question through conducting limb/gait video analysis of the 6 points of interest on a mouse's hind legs, including the Iliac crest, hip, knee, ankle, foot, and toe regions.

PROTOCOL/METHODS

This protocol was adopted by Fiander and others ¹ to analyze the video recordings of several of mice over the course of a specific timeframe, with frequent modifications and additions to the initial setup.

3D MARKERS

1. Prepared 100 to 200 3D marker print outs to place on the hind legs for each mouse

2. Use tweezers to cut away the excess support surrounded by the print outs
3. Use Aluminum weighing dish to dispense adhesive glue that will be used to place markers on mice

ANIMAL PREPARATION FOR VIDEO RECORDING

1. Set up stereotax and nose nozzle that is required to keep the mouse down during preparation
2. Use heating pad that is heated up to 37 degrees celsius because mice will lose body heat under anesthesia
3. Connect the oxygen plug to the oxygen tank, and connect the vacuum plug to the vacuum tank. The oxygen is used to dilute the isoflurane, while the vacuum is used to suck out redundant isoflurane leaking from the tube joint
4. Oxygen tube is suggested to be up to level 20, while the vacuum tube is suggested to be up to level 30
5. Anesthetize the mouse with isoflurane gas
6. Once the mouse is out, attach his nose to the tube in order for him to stay under during preparation
7. Apply eye gel to eyes so that retina will not dry out
8. Shave desired side of hind legs to apply the 3D markers used for motion tracking

9. Apply 3D markers to the six points of interest: iliac crest, hip, knee, ankle, foot, and toes

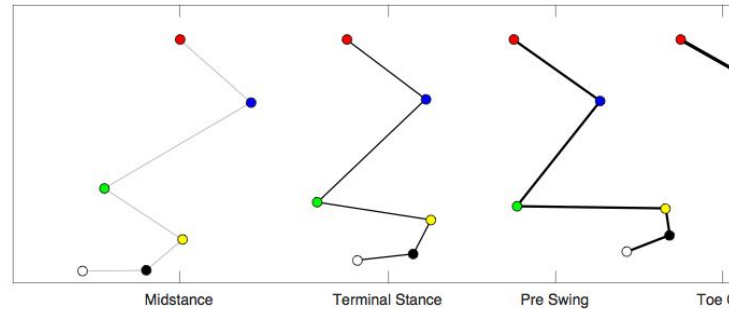
LOCOMOTION RECORDING

1. Setup high definition camera; adjust the exposure time, aperture, light source, gain, and black level
2. Design wheel that allows for video recording for the side view of where the 3D markers are located
3. Position camera at the same height and level as the custom made wheel
4. Adjust LED speed monitor approximately 2 millimeters from wheel to obtain speed data
5. Select ideal number of frames that is relative to seconds
6. Begin recording the mouse until 10 to 15 consecutive steps have been achieved on each trial
7. Once recording is complete, turn off camera and return mouse to its cage. Clean wheel off with 90% ethanol to reduce the stress levels of each mouse

VIDEO ANALYSIS

1. Upload and crop videos using the computer software program ImageJ
2. Enable a good blob diameter and threshold to manually track the 6 points of interest
3. Set filters on the X and Y coordinates to eliminate access diameter points

4. Go through video frame by frame to catch any missed diameter points
5. Export all statistics to microsoft excel
6. Identify the start and ending of each gait cycle based on the toe off
7. Use statistics to plot out angle averages using computer software program MATLAB
8. Go through video frame by frame to derive the number of pixels needed to convert pixels to centimeters to obtain stride length
9. Multiply the start and ending of the gait cycle, then divide by the number of frames in each pixel to obtain the stride frequency

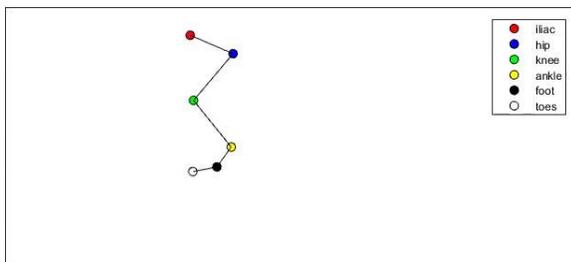


B.

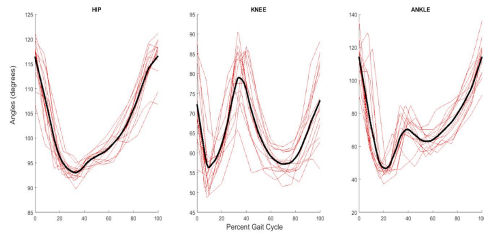
In graph (A), we derived these coordinates from a motion tracking video program MATLAB, which will help us to analyze the hip, ankle, and knee joints. In graph (b) we show the steps that are needed for a completed gait cycle, which includes the Midstane, Terminal Stance, Pre Swing, Toe Off, Mid Swing, and Foot Flat.

EXPERIMENTAL DATA

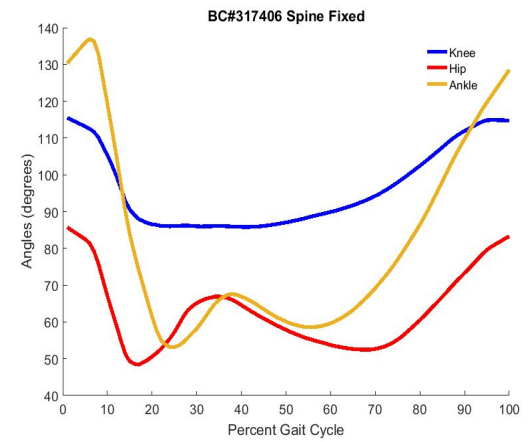
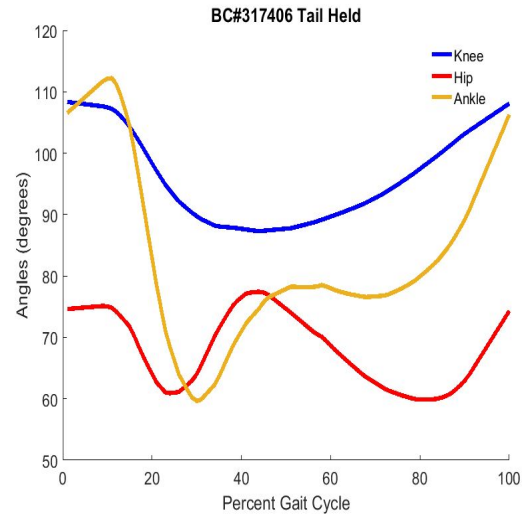
A.



C.

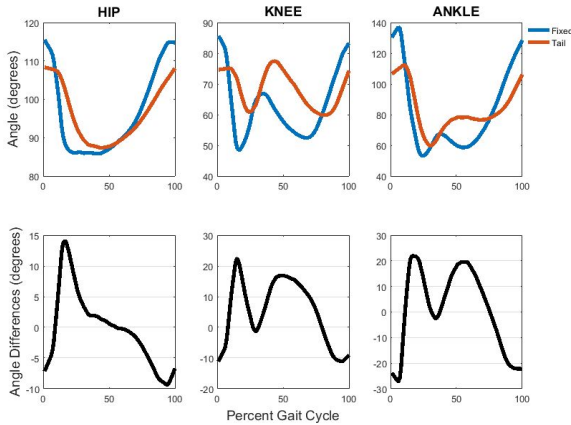


In graph (C) we averaged the hip, knee, and ankle joints to one single gait cycle, which is derived from 10 to 15 normalized steps that the mouse has taken in a single recording



D.

In graphs (D) the knee is represented by the blue line, the hip is represented by the red line, and the ankle is represented by the yellow line. We compared our tail-held and spine fixed averages of the gait cycle, and we noticed that there was a general trend that each angle followed.



E.

Although there is a general trend in the joint angles, in graph (E) we determined that there is a difference in angles that is no more than 20 °.

RESULTS/DISCUSSION

The Parameters that we measured during this study, includes the stride length, stride frequency, range of motion, RMS difference of angles, video velocity, distance traveled, percent time moving, average moving velocity, and maximum velocity.

We performed a T-test on all ratios of the parameters, and derived each of the specific P-values,

Parameter (RATIO)	P-Value
Stride Length	0.260
Stride Frequency	0.0832
Video Velocity	0.169
RMS Differences <ul style="list-style-type: none"> ● Hip ● Ankle ● Knee 	<ul style="list-style-type: none"> ● 0.299 ● 0.125 ● 0.0295
Range of Motion <ul style="list-style-type: none"> ● Hip ● Ankle ● Knee 	<ul style="list-style-type: none"> ● 0.0304 ● 0.0324 ● *0.252
Total Distance Traveled	*0.0040
Percent Time Moving	0.0659
Average Moving Velocity	*0.0201
Maximum Velocity	*0.0005

The P-Values that are labeled with a *Star* indicates that the locomotive patterns between the ratio of tail-held and spine-fixed mice are significant, while the parameters without the star, indicates the the locomotive patterns are not significantly different. Although statistically, we can see that there is a change in patterns, it is vital to understand that each mouse is different, and many circumstances will affect the locomotion of a mouse.

CONCLUSION

In summary, we have developed a method for awake spinal cord imaging without inhibiting a mouse's gait cycle, and developed a motion tracking protocol using computer software programs like MATLAB and IMAGEJ. Steps that should be taken in the future includes increasing the time it takes to train each mouse, finding a routine structure that enables us to accurately place the 3D Markers on the desired points of interest, and finding different adhesive glues that will not irritate the mice, which in turn will affect how they walk. We can say with confidence that neural activity in locomoting mice is likely to accurately represent the activity of locomotor neural circuits in freely behaving mice.

REFERENCES

1. Kiehn, Ole (2016) Decoding the organization of spinal circuits that control locomotion (Vol. 17)
2. Drew, T. & Marigold, D. S. Taking the next step: cortical contributions to the control of locomotion. *Curr. Opin. Neurobiol.* 33, 25–33 (2015).
3. Takakusaki, K. Neurophysiology of gait: from the spinal cord to the frontal lobe. *Mov. Disord.* 28, 1483–1491 (2013).
4. Garcia-Rill, E. The basal ganglia and the locomotor regions. *Brain Res.* 396, 47–63 (1986).
5. Grillner, S. & Robertson, B. The basal ganglia downstream control of brainstem motor centres — an evolutionarily conserved strategy. *Curr. Opin. Neurobiol.* 33, 47–52 (2015).
6. Garcia-Rill, E., Hyde, J., Kezunovic, N., Urbano, F. J. & Petersen, E. The physiology of the pedunculopontine nucleus: implications for deep brain stimulation. *J. Neural Transmission* 122, 225–235 (2015).
7. Ryczko, D. & Dubuc, R. The multifunctional mesencephalic locomotor region. *Curr. Pharm. Design* 19, 4448–4470 (2013).
8. Dubuc, R. et al. Initiation of locomotion in lampreys. *Brain Res. Rev.* 57, 172–182 (2008).
9. Orlovsky, G. N., Deliagina, T. G. & Grillner, S. *Neuronal Control of Locomotion. From Mollusc to Man* (Oxford Univ. Press, 1998).
10. Jordan, L. M., Liu, J., Hedlund, P. B., Akay, T. & Pearson, K. G. Descending command systems for the initiation of locomotion in mammals. *Brain Res. Rev.* 57, 183–191 (2008).
11. Kiehn, O. Locomotor circuits in the mammalian spinal cord. *Annu. Rev. Neurosci.* 29, 279–306 (2006).
12. Grillner, S. The motor infrastructure: from ion channels to neuronal networks. *Nat. Rev. Neurosci.* 4, 573–586 (2003).
13. Matthew J Farrar, Ida M Bernstein, Donald H Schlafer, Thomas A Cleland, Joseph R Fetcho & Chris B Schaffer (2012). *Chronic in vivo imaging in the mouse spinal cord using an implanted chamber* (Vol. 9)

Mapping the Functional Organization of the Zebrafish Hindbrain Using Light-Sheet Microscopy

Rick Zirkel¹, Joseph Fetcho², Xinyue Cui²

¹SUNY University at Buffalo, Amherst, NY, ²Cornell University, Ithaca, NY

I. Abstract

Zebrafish have features that offer the possibility of revealing underlying principles of neuronal functionality that apply across all vertebrates. Our work focused on the organization of the neurons in the hindbrain. Earlier work revealed columns of neurons in hindbrain that differed in structure and neurotransmitter. We set out to use light sheet microscopy to determine functional patterning of these columns. We asked whether neurons with similar activity patterns are arranged in columns ordered by age. From light sheet calcium imaging, neurons were correlated by waveform to others within the hindbrain, thereby showing the distribution of neurons with similar function. Data was also analyzed to determine if cells showed similar functionality dorsal-ventrally, to test possible organization by neuronal age, which maps along the dorsoventral axis of hindbrain. The data revealed broad columnar patterning in the hindbrain that likely underlies many behaviors. The data also indicated that neurons at similar dorsoventral locations share activity patterns, supporting a broad functional organization based on age.

II. Introduction

The zebrafish has become a fundamental part of our ability to explore and understand the complexities of the vertebrate brain. With the use of such an animal model we have been able to advance research in many ways due to its advantageous characteristics. At a young age, the zebrafish larvae are small and transparent, allowing us to see into the spinal cord and brain with ease. The fish are also genetically accessible, so we are also able to create transgenic lines of the animal with calcium sensors, which make it possible to monitor neuronal activity.³

Until recently, point-scanning methods such as confocal and 2-photon microscopy were the

preferred technology available to image the entire brain. These methods were very slow and inefficient for examining how the brain works as a whole. Due to recent technological advances, however, light-sheet microscopy has improved the efficiency of whole brain imaging with a method 100-1000 faster than point-scanning. Light-sheet microscopy provides fast data collection by imaging in small-width sheets. For our purposes, 5 μ m sheets of images were recorded, while the laser and objective moved rapidly up and down to cover the entire brain. These sheets are then stacked on top of each other in order to construct a whole-brain image. This method is extremely fast as it produces whole-brain image data at about 1 brains/sec.⁴

Our experiments used light-sheet microscopy in order to image the hindbrain of 4-6 dpf (days post fertilization) zebrafish larvae. The hindbrain is important as it is where a lot of circuits for control of movement are located, including circuits for eye, jaw and body movements. It was found in previous research that the neurons in the hindbrain of the larval zebrafish form columns based on different neuronal morphologies and neurotransmitters, with the columns extending through hindbrain. Figure 1 shows a top view of these hindbrain columns. Figure 2 shows cross sections of the hindbrain stained for different markers. These markers form columns that run through hindbrain, which contain particular neuron types, suggesting that there is a columnar organization of the hindbrain structurally. We set out to ask whether there is evidence for this columnar organization functionally as well.

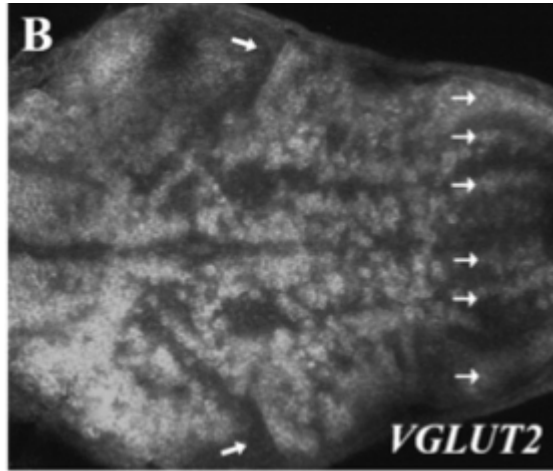


Figure 1: Top view of the zebrafish brains with arrows on the right side indicating the columns that run through the hindbrain.¹

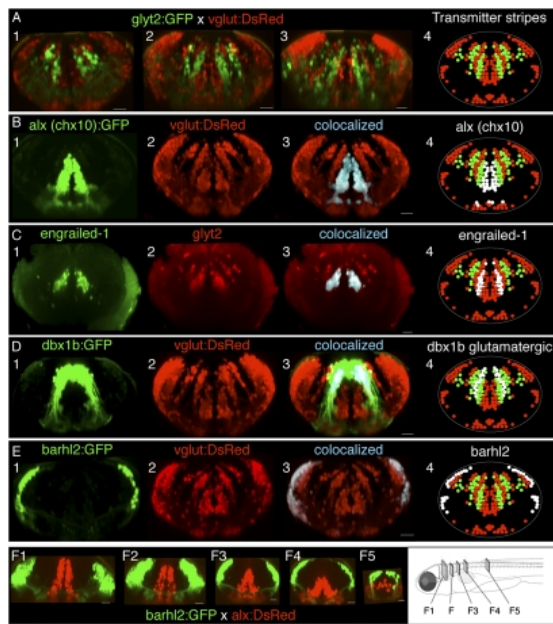


Figure 2: Cross sections of the larval zebrafish hindbrain indicating columnar patterning by transgenic markers.²

Another aspect of the hindbrain our work focused on was an existence of functional age patterning along the dorsal-ventral axis. Earlier research shows a structural age patterning in the columns of the hindbrain, as well as a functional patterning within circuits involved in swimming. These studies showed that older neurons are located

more ventral and are associated with big, powerful movements, while younger ones are more dorsal, and are used for finer movements. We set out to determine if this functional patterning extends to all different behaviors associated with columns of neurons in the hindbrain.²

Thus, there were two key questions that our work addressed. The first was whether the columns of the hindbrain contained functionally similar neurons, and second was whether neurons of similar age also share similar functional roles. We predicted that if we could monitor activity on the whole brain scale, neurons that have similar activity patterns would form columns in the hindbrain. Further, we expected neurons that are at similar positions from the top to the bottom of the brain would have similar activity patterns. With the use of fast, whole-brain imaging through light-sheet microscopy, we were able to test these predictions.

III. Materials and Methods

We were in a position to test our predictions because of the recent development of high-speed imaging through light-sheet microscopy. For our purposes of imaging activity in the hindbrain, we used 4-6 dpf fish of transgenic line Casper HUC:H2B GCamp6f. Several steps were required in order to collect the necessary data.

Between 8-10 fish of the desired line were screened using a fluorescence dissecting scope to determine if the calcium indicator was present in the neurons of the fish and bright enough to provide a sufficient fluorescence output during activity. The positive fish were then given a health evaluation in order to assess the viability of the fish for experimental use. We looked for fish with strong blood flow with no occlusions, as well as no visible deformities. From this filtered group of fish, on each experimental trial one was separated. This fish was then paralyzed using the neurotoxin bungarotoxin. The fish was isolated in the toxin for 4-5 minutes, returned to regular solution, and monitored for up to 10 minutes to determine the effectiveness of the drug. If the fish was completely immobilized and still in good health, it was ready to be prepared for imaging.

The fish was then embedded in a 2% agar solution at a particular orientation. A block of agar containing the fish was then mounted onto a stand in a 3D printed chamber that allows the laser light to reach the sample from the left, and for the camera to record the fluorescence from above. This chamber was placed in the laser apparatus, which utilized a 488 nm laser to excite the GFP calcium indicator protein. We collected activity of the fish by letting the fish do different behaviors with no stimulation for 10 minutes, imaging at a brain per second. This allowed us to look at the spontaneous activity pattern of each neuron over time.

These stacks of hundreds of brains were then processed to allow us to register and extract the images of the neurons in the brain. First, the initial images were filtered to remove background so that only the pixels that had sufficient fluorescence intensity were registered. This cut down processing and registration time significantly. We were then able to overlap the images and determine if the fish drifted at all during the data collection, which could then be corrected.

We then inputted the raw fluorescence data into Imaris software. From this we were able to localize the fluorescence to individual regions in the brain. From this initial plot, we then used several filters to eliminate potential extraneous data that could be mistaken for cells. From this we were able to segment the fluorescence to individual neurons, whose intensity we could track through a whole time series of brains to get fluorescence changes over time.

The first experiment that was conducted used 4-day old fish embedded in a dorsal-up position (Figure 3). Further experiments were conducted with fish mounted at different orientations for validation purposes. Fish were imaged at 45 and 90 degree tilts toward the laser (Figure 4, Figure 5). Sets of images were collected at these angles to show that the conclusions were not altered by the orientation of the fish, which might influence correlation patterns because of the orientation of the light sheets relative to the neurons.

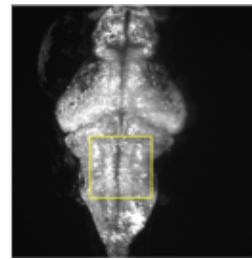


Figure 3: Single-plane image of dorsal-up fish.

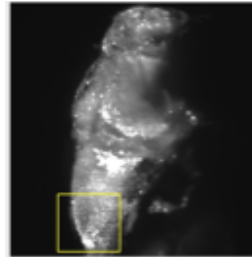


Figure 4: Single-plane image of fish angled at 45 degrees toward laser.

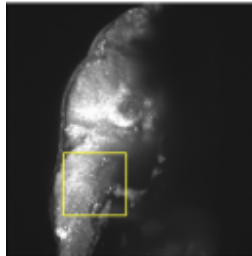


Figure 5: Single-plane image of fish angled at 90 degrees toward laser.

IV. Results and Discussion

From the data we collected in the first type experiment with the dorsal-up fish, we were able to examine our first question of whether or not cells in hindbrain columns have similar patterns of activity to one another, which would allow us to identify columns functionally.

We were able to analyze cells in a LabView program. Through the program we were able to plot the cells on a 3D trace and visualize the neurons individually to see their waveform and fluorescence intensity. Waveform traces are shown as fluorescence vs time. The highest correlated clusters of cells based on comparisons of their calcium signal waveforms, and therefore function, were found. Groups of highly correlated cells of different functionality were color coded and plotted. (Figure 6). These cells were often organized into columns extending from rostral to caudal in the brain.

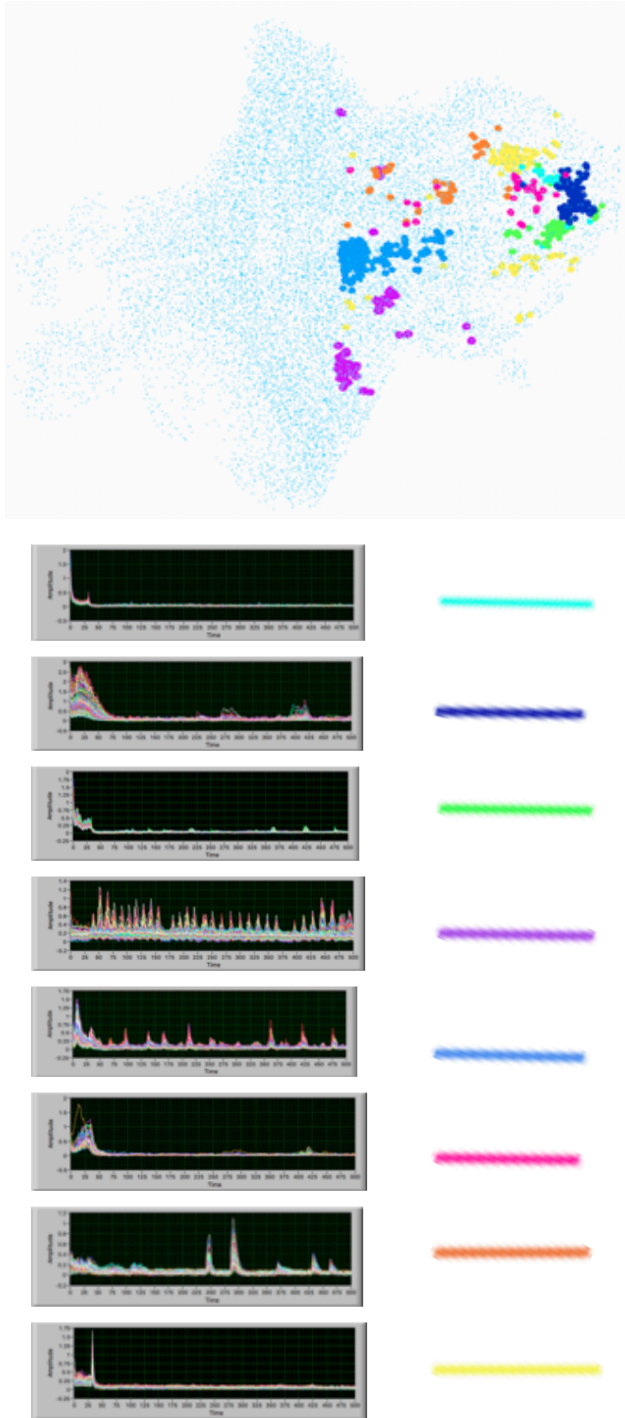


Figure 6: 3D plot highlighting highly correlated cell clusters, indicated by colors. The waveforms of each cluster were indicated by a color key.

Therefore, the answer to the first question we asked was that we saw a functional organization into columns in some sets of cells, so there is a

columnar functional organization that we revealed with light-sheet microscopy.

We were also able to examine the second question which asked if there is a functional patterning in the dorsal-ventral axis of the brain. If there is functional order by age, then we expected cells that are nearby one another along the axis would have similar activity patterns. We used a strategy that color codes cells based on correlation patterns. We explored the correlation patterns from top to bottom, as is shown in Figure 7, by plots in which cells that have high correlations have similar colors in cross sections of the brain. This revealed that there are high correlations among neurons close together along the dorsoventral axis, since the colors are patterned dorsal-ventrally. (Figure 7)

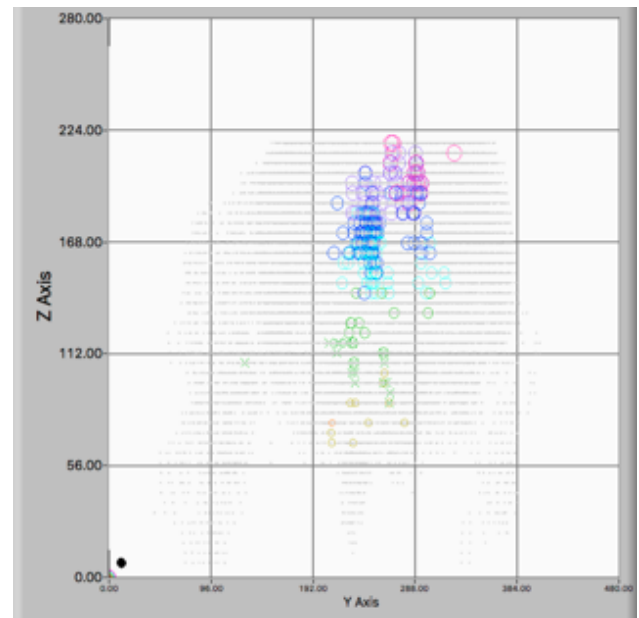


Figure 7: Plot showing the functional correlation pattern that maps onto dorsal-ventral position and therefore age.

V. Conclusion

Based on our data, we were able to provide evidence supporting our predictions our work set out to examine. With respect to a functional organization of the columns in the hindbrain, the data revealed broad columnar patterning that likely underlies many behaviors. For a functional organization by age

along the dorsal-ventral axis in columns, the data indicated that neurons at similar locations along the axis share activity patterns, supporting a broad functional organization based on age. Further experimentation and statistical analysis of such conclusions must be executed in order to validate our findings.

The purpose of determining the organization of the hindbrain is to develop a more complete understanding of the functional organization of the brain. The similarity between vertebrate brains makes it likely that the patterned we revealed will be shared by other vertebrates, including humans, which would make them fundamental principles of the organization of the brain.

VI. Acknowledgments

I'd like to thank Dr. Joseph Fetcho for his support and mentorship throughout my time in his lab. I would also like to thank Kimberly McArthur and Xinyue Cui for their help in developing my skills and knowledge of working with zebrafish and light-sheet microscopy, as well as the rest of the Fetcho Lab for making me feel welcome this summer. Finally, I would like to thank the NSF NeuroNex Initiative for funding this project.

VII. References

1. Higashijima, S. , Mandel, G. and Fetcho, J. R. (2004), Distribution of prospective glutamatergic, glycinergic, and GABAergic neurons in embryonic and larval zebrafish. *J. Comp. Neurol.*, 480: 1-18.
doi:[10.1002/cne.20278](https://doi.org/10.1002/cne.20278)
2. Kinkhabwala A, et al. A structural and functional ground plan for neurons in the hindbrain of zebrafish. *Proc Natl Acad Sci USA*. 2011;108:1164–1169.
3. Adam Michael Stewart, Oliver Braubach, Jan Spitsbergen, Robert Gerlai, Allan V. Kalueff, *Zebrafish models for translational neuroscience research: from tank to bedside*, *Trends in Neurosciences*, Volume 37, Issue 5, 2014, Pages 264-278, ISSN 0166-2236, <https://doi.org/10.1016/j.tins.2014.02.011>.

4. Michael Weber, Michaela Mickoleit, Jan Huisken, Chapter 11 - Light sheet microscopy, Editor(s): Jennifer C. Waters, Torsten Wittman, *Methods in Cell Biology*, Academic Press, Volume 123, 2014, Pages 193-215, ISSN 0091-679X, ISBN 9780124201385, <https://doi.org/10.1016/B978-0-12-420138-5.00011-2>.